Multiple-spin effects in fast magic angle spinning Lee-Goldburg cross-polarization experiments in uniformly labeled compounds

Ladizhansky, V.; Vinogradov, S.; Rossum, B.J. van; Groot, H.J.M. de; Vega, S.

Multiple-spin effects in fast magic angle spinning Lee–Goldburg cross-polarization experiments in uniformly labeled compounds

Cite as: J. Chem. Phys. **118**, 5547 (2003); https://doi.org/10.1063/1.1517299
Submitted: 10 July 2002 . Accepted: 06 September 2002 . Published Online: 07 March 2003

V. Ladizhansky, E. Vinogradov, B.-J. van Rossum, H. J. M. de Groot, and S. Vega

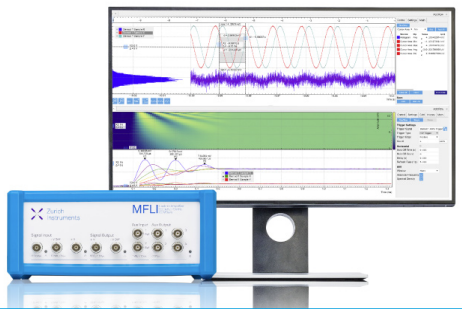

Multiple-spin effects in fast magic angle spinning Lee–Goldburg cross-polarization experiments in uniformly labeled compounds

V. Ladizhansky[a] and E. Vinogradov
Chemical Physics Department, Weizmann Institute of Science, 76100 Rehovot, Israel

B.-J. van Rossum[b] and H. J. M. de Groot
Leiden Institute of Chemistry, Gorlaeus Laboratories, Leiden University, P.O. Box 9502, 2300 RA Leiden, The Netherlands

S. Vega[c]
Chemical Physics Department, Weizmann Institute of Science, 76100 Rehovot, Israel

(Received 10 July 2002; accepted 6 September 2002)

The proton–carbon polarization exchange in Lee–Goldburg cross-polarization magic angle spinning (LG-CP MAS) nuclear magnetic resonance experiments on uniformly ^{13}C-labeled compounds at high spinning frequency is studied. It is shown that the multiple carbon labels in the samples greatly influence the spin dynamics during the LG-CP mixing times. The zeroth order effective LG-CP MAS spin Hamiltonian is a sum of zero quantum dipolar interaction terms. These pairwise dipolar terms generally do not commute with each other, making it impossible to factorize the evolution operator. Consequently, the frequencies of the dipolar oscillations as well as the polarization transfer amplitudes become strongly dependent on the configuration of the spins involved in the multiple heteronuclear couplings. The strong carbon–proton couplings usually attenuate polarization transfers between weakly coupled spins. In practice, this implies that except for strongly coupled or isolated heteronuclear ^{13}C–^{1}H spin pairs, it is difficult to unambiguously extract structural constraints from experimental data. To better understand the complexity of the LG-CP processes, experiments on simple three- and four-spin systems are simulated and analyzed. More specifically, it is shown that in ^{13}CH–^{13}CH and $^{13}CH_2$–^{13}C spin systems, a significant amount of the proton polarization can be transferred to both carbons, despite the fact that the individual proton–carbon heteronuclear couplings between each proton and the carbon spins are very different. The dependence of the polarization transfer on the position of the proton carrier frequency is analyzed and it is shown that by an appropriate choice of this frequency, specific polarization transfer pathways can be selected. Experimental results from [U–^{13}C] tyrosine.HCl and [U–^{13}C, ^{15}N] histidine.HCl.H_2O samples are in satisfactory agreement with simulations. © *2003 American Institute of Physics.* [DOI: 10.1063/1.1517299]

I. INTRODUCTION

Cross polarization[1] (CP) is one of the main components of almost all solid state NMR experiments. The combination of the CP methodology with magic angle spinning[2,3] (MAS) and high power heteronuclear decoupling,[4] in particular, two pulse phase modulation (TPPM) decoupling,[5] makes it possible to obtain high resolution ^{13}C and ^{15}N spectra.

Historically, the cross polarization exchange process in static solids has been described from a thermodynamic point of view.[6,7] This description was extended to high spinning CPMAS experiments by Meier.[8] Recently, a different approach for analyzing the cross polarization process has been investigated, based on the coherent time evolution of a spin system consisting of a single carbon spin coupled to many protons.[9] Signal enhancements were evaluated[10] by following the spin dynamics in these multispin systems under moderate and fast sample spinning, and the results agreed well with experimentally observed signals.[11,12]

This approach proved to be particularly valuable for interpreting the Lee–Goldburg decoupled version of the cross-polarization experiment (LG-CP). In this experiment, proton–proton interactions are largely suppressed by applying an off-resonance RF field that results in an effective field pointing along an axis tilted by the magic angle with respect to the direction of the external field.[13] At the same time, the heteronuclear carbon–proton dipolar interaction is reintroduced via a Hartmann–Hahn condition imposed on the effective RF fields experienced by the nuclei.[14] In particular, van Rossum *et al.*[11] applied LG-CP to measure C–H interactions in a uniformly ^{13}C-labeled tyrosine sample by analyzing CH buildup curves. An easy interpretation of such data is only possible for strongly coupled or spatially isolated CH spin pairs. In other cases the spin dynamics are more complicated and should be analyzed by considering larger spin clusters.

[a]Present address: Francis Bitter Magnet Laboratory, Massachusetts Institute of Technology, NW 14-4115, Cambridge, Massachusetts 02139.
[b]Present address: Forschungsinstitute für Molekulare Pharmakologie (FMP), Robert-Rosle Str. 20, D-13125 Berlin, Germany.
[c]Author to whom correspondence should be addressed. Electronic mail: shimon.vega@weizmann.ac.il

The LG-CP spin dynamics in naturally abundant alanine is described in Ref. 12, where it is shown that for the successful interpretation of the experimental carbon signal enhancements, it was indeed necessary to consider multiple carbon–proton interactions. However, a relatively small number of protons was sufficient to describe the carbon–proton spin dynamics. By and large six protons coupled to one carbon are enough to adequately characterize the polarization of carbons at natural abundance.

The situation becomes much more complicated in uniformly ^{13}C-labeled systems, where the spin system becomes a continuous network of dipolar-coupled heteronuclear-spins. Strongly coupled ^{13}C–H spin pairs can be in proximity to each other, and the time-dependent growth of each carbon signal can be influenced by proton–carbon interactions with adjacent spin pairs. Effects of this type were first observed experimentally by van Rossum *et al.*[11] and are analyzed theoretically here.

Note that some of the effects observed in these experiments, as well as in Ref. 12, are a manifestation of dipolar truncation previously observed in homonuclear recoupling experiments.[15–19] This truncation causes a reduction of the polarization transfer efficiency between weakly coupled homonuclear spin pairs, when at least one of the interacting spins is strongly coupled to a third spin. These and similar effects were observed and analyzed by Costa,[15] Howhy *et al.*,[16] Brinkmann *et al.*,[17] Glaser *et al.*,[18] and Hodgkinson *et al.*[19]

Herein, we will focus on the multispin dynamics occurring during LG-CP experiments.[11] At sufficiently high spinning frequencies the proton–carbon polarization transfer can be adequately described by an effective time-independent zero-quantum (ZQ) heteronuclear dipolar Hamiltonian.[12] Fourier transformation of the carbon buildup results in CP-line-shapes with spectral singularities that are characteristic for the strongest carbon–proton interactions in the spin system.[11]

We will show that the behavior of the carbon signals is a manifestation of the coherent nature of the polarization transfer processes during the LG-CP process. Although all experimental data are analyzed using simulations, the main features of the spin dynamics are retained in small three-spin and four-spin systems. Our analytical description will therefore mainly concentrate on analyzing small spin systems that can be solved either precisely or with some reasonable approximations. The details of the theoretical calculations are presented in the EPAPS material,[33] whereas the results are discussed in the main text in the context of the experiments.

II. EXPERIMENTAL AND SIMULATIONS

The pulse sequences used for our 2D and 3D experiments are shown in Fig. 1. Figure 1(a) represents the pulse sequence of the basic LG-CP experiment. Here, the first ''magic'' pulse aligns the proton magnetizations in the direction of the LG effective field. These magnetizations are then locked along that direction, while a RF field is applied to the carbons satisfying the first Hartmann–Hahn condition. A schematic representation of the 3D LG-CP MAS experiment is shown in Fig. 1(b). In this experiment the proton magnetizations are first flipped down by a 90° pulse to a direction perpendicular to the effective phase modulated Lee–Goldburg (PMLG) field and then allowed to evolve during a time t_1 according to their scaled chemical shift values. During this evolution the homonuclear proton–proton dipolar couplings are suppressed by either PMLG (Refs. 20–22) irradiation with 9 pulses per half a cycle (PMLG-9) or frequency switched Lee–Goldburg (FSLG) irradiation.[23,24] Following the evolution in the t_1-domain, the proton magnetizations are brought first to the xy-plane and then one of their components is locked in the direction of the effective LG proton field. During the LG-CP period τ the LG RF field markedly suppresses the homonuclear dipolar couplings and the growth of the carbon polarization is solely governed by the heteronuclear proton–carbon dipolar interaction.

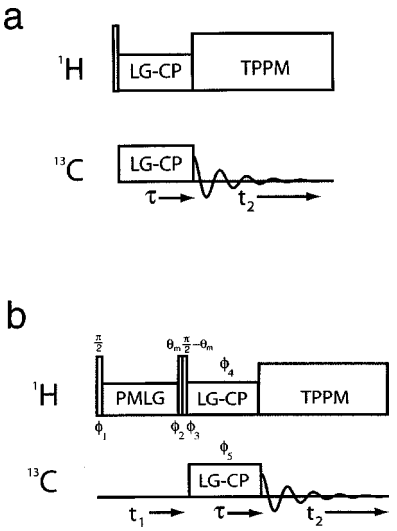

FIG. 1. Pulse sequences for 2D LG-CP (a) and 3D LG-CP (b) experiments. The phases of the 3D LG-CP experiment were $\varphi_1=x$, $\varphi_2=y$, $\varphi_3=-y$, $\varphi_4=x$, and $\varphi_5=x$. The phases of the pre-LG-CP pulse (φ_3) and the LG-CP proton locking pulse (φ_4) were incremented according to the TPPI scheme.

The spectra were acquired on a DSX-300 and a DRX-600 Bruker spectrometer equipped with 4 mm double resonance Bruker probes. The experiments at 300.13 MHz proton field were performed on a sample of [U–^{13}C, ^{15}N] histidine.HCl.H_2O, and the PMLG-9 sequence was used for the homonuclear decoupling. The experiments at 600.13 MHz were performed on a sample of [U–^{13}C] tyrosine.HCl with FSLG as the decoupling scheme. The spinning frequencies used during the experiments were 10 kHz on the DSX-300 spectrometer and 12 kHz on the DRX-600 spectrometer. For achieving better B_1 homogeneity, the samples were confined to the middle part of the rotor by spacers.

The experimental parameters for the measurements on the DSX-300 spectrometer are as follows. The proton power for the PMLG-9 homonuclear decoupling was 81 kHz and the pulses had a length of 1.1 μs. The phases of these pulses are given elsewhere.[20] The proton and carbon RF powers used for the LG-CP experiments were 78.77 kHz and 85.9 kHz, respectively. The experimental parameters for the measurements on the DRX-600 spectrometer were reported previously.[11]

The phases of the (pre-LG-CP) $90°-\theta_m$ pulse and the

LGCP proton-locking pulse were varied according to the standard time proportional phase incrementation (TPPI) scheme.[25] ^{13}C LG-CP buildup curves were deduced from Fourier transformed 2D experimental spectra by evaluation of the volume integrals of individual ^{1}H–^{13}C cross peaks.

The numerical simulations were performed using the SIMPSON (Ref. 26) and SPINEVOLUTION (Ref. 27) software packages. For the analysis of the experimental data the atomic coordinates of histidine.HCl.2H_2O and tyrosine. HCl were downloaded from the Cambridge Database, and the chemical shift values were taken from the 1D proton and carbon spectra.

III. THEORY

A. The zero order spin Hamiltonian

In our discussion we will use the operators I_p and S_p, with $p=x,y,z$, denoting proton and carbon spin operator components, respectively. The rotating frame LG-CP MAS Hamiltonian, which describes the cross-polarization process in an I_kS_m system of k protons $I=1/2$ and m carbons $S=1/2$, can be written as

$$H(t)=-\omega_{1I}I_x+\sum_i \Delta\omega_i I_{iz}-\omega_{1S}S_x+\sum_{i,j} b_{ij}(t)I_{iz}S_{jz}. \tag{1}$$

The first two terms represent the RF irradiation field and the off-resonance values of the protons, respectively, and the third term is the RF field on the carbons at resonance. The last term describes the heteronuclear proton–carbon interactions with coefficients that are time-dependent due to sample spinning. Assuming that the homonuclear carbon–carbon interaction terms are small compared with the carbon RF field and are averaged by the sample spinning, and that the carbon offset terms are also much smaller than this RF term, these two interactions can be omitted from the Hamiltonian. The $b_{ij}(t)$ coefficients are proportional to the heteronuclear dipolar coupling parameters $\omega_d^{(i,j)}=(\mu_0/4\pi)(\gamma_C\gamma_H\hbar/r_{ij}^3)$ and can be expressed as[28]

$$b_{ij}(t)=2\omega_d^{(i,j)}\sum_{n=-2}^{2} G_n^{(i,j)}\exp\{in\omega_R t\} \tag{2}$$

with $G_n^{(i,j)}$ geometric coefficients depending on polar angles θ_{ij} of the distance vector r_{ij}, connecting the positions of the interacting spins in the rotor frame, and on the magic angle $\theta_m=54.7°$.

The ω_{1I} and ω_{1S} values in Eq. (1) must fulfill two conditions: the LG condition, requiring that the proton off-resonance value is $\Delta\omega_i=\omega_{1I}\tan^{-1}\theta_m$, assuring suppression of the homonuclear proton–proton dipolar couplings, and the Hartmann–Hahn condition, requiring that the effective field $\omega_{\text{eff}\,i}=\sqrt{\omega_{1I}^2+\Delta\omega_i^2}$ on the protons is different from the RF field on the carbons by an integer number n times the spinning frequency $\omega_{\text{eff}\,i}-\omega_{1S}=n\omega_R$, with $n=-2,-1,1,2$. This enables an efficient polarization transfer between proton and carbon spins. However, these conditions cannot be fulfilled simultaneously for all protons due to their chemical shift dispersion. A slight deviation from the LG condition reintroduces some small effective homonuclear proton–proton interactions. However, this does not have an appreciable effect on the LG-CP buildup curves at high spinning frequencies, as was shown earlier.[12] It is therefore reasonable to ignore the proton–proton interactions in Eq. (1). It is impossible to satisfy the Hartmann–Hahn condition for all protons at the same time, since the effective fields experienced by protons with different chemical shifts are dissimilar. As will be discussed later, these mismatched conditions will have a significant effect on the signal enhancement of carbons in weakly coupled heteronuclear spin pairs. To describe these effects, we introduce an average offset value $\Delta\omega=\omega_{1I}\tan^{-1}\theta_m$ that is determined by ω_{1I} according to the exact LG condition, and a set of off-resonance deviations $\delta\omega_i=\Delta\omega_i-\Delta\omega$. The average effective proton field ω_{effI} points in the direction of the magic angle in the $\Delta\omega$-rotating frame and satisfies the Hartmann–Hahn condition,

$$\sqrt{\omega_{1I}^2+\Delta\omega^2}=\omega_{\text{eff}\,I}=\omega_{1S}+n\omega_R. \tag{3}$$

Thus, the deviation from the exact matching condition for each proton is solely determined by its $\delta\omega_i$ value. Assuming that the $\delta\omega_i$ off-resonance deviations are much smaller than the average $\Delta\omega$ offset value, the protons with specific $\delta\omega_i$ values will be mismatched from the HH condition by an amount $\sim\cos\theta_m\delta\omega_i$.

In the doubly tilted frame of the off-resonance value $\Delta\omega$, where the average effective fields are pointing in the z-direction, the Hamiltonian has the form

$$H_0(t)=\sum_{i,j} -\omega_{\text{eff}\,I}I_{zi}-\omega_{1S}S_{zj}-\delta\omega_i(\sin\theta_m I_{ix}-\cos\theta_m I_{iz}) + \sin\theta_m b_{ij}(t)I_{ix}S_{jx}-\cos\theta_m b_{ij}(t)I_{iz}S_{jx}. \tag{4}$$

To derive a zero-order average Hamiltonian from Eq. (4), we first transform $H_0(t)$ to the interaction frame, defined by the transformation operator

$$U(t)=\exp\{-i(\omega_{\text{eff}\,I}I_z+\omega_{1S}S_z)t\}. \tag{5}$$

In this interaction representation all dipolar terms oscillate with frequencies $n\omega_R\pm\omega_{1S}$ or $n\omega_R\pm(\omega_{\text{eff}\,I}\pm\omega_{1S})$, the I_{ix} off-resonance terms oscillate with $\omega_{\text{eff}\,I}$ and the I_{iz} terms stay time-independent. At one of the Hartmann–Hahn conditions, $\omega_{\text{eff}\,I}-\omega_{1S}=n\omega_R$, some of these terms become time-independent and take the form

$$\bar{H}=\sum_{i,j}\bar{H}_{ij}+\sum_i \delta\omega_i\cos\theta_m I_{iz},$$

$$\bar{H}_{ij}=\frac{\omega_d^{(i,i)}\sin\theta_m}{4}G_n^{(i,j)}[I_i^+S_j^-\exp(in\phi_i) + I_i^-S_j^+\exp(-in\phi_i)]. \tag{6}$$

The spin dynamics of the I_nS_m system will primarily be governed by this average Hamiltonian as long as the spinning frequency is sufficiently high, $\omega_R\gg(\omega_d^{(i,j)}|G_n^{(i,j)}|/4)\sin\theta_m$, and $\delta\omega_i\ll\Delta\omega$. Thus during the LG-CP mixing time τ of the 3D LG-CP experiment, the Hamiltonian of Eq. (6) can be used to estimate the flow of polarization between the spins. For each τ value a 2D ^{13}C–^{1}H chemical shift correlation spectrum can be generated with cross peaks at

$(\omega_i^I,\ \omega_j^S)$, where ω_i^I and ω_j^S are the chemical shifts of the I and S-spins, respectively. These 2D spectra allow us to separate the contributions of different protons to the initial density matrix at $\tau=0$. The buildup of the cross peak $(\omega_i^I,\ \omega_j^S)$, governed by the effective Hamiltonian $\bar{H}$ in Eq. (6), corresponds to the polarization transfer from the proton i to the carbon j. For each τ value the integrated intensities $S_{ij}(\omega_i^I,\omega_j^S;\tau)$ of the cross peaks at positions $(\omega_i^I,\ \omega_j^S)$ in the 2D spectra are equal to[12]

$$S_{ij}(\omega_i^I,\omega_j^S;\tau)=\gamma_I\int d\Omega\ \mathrm{tr}\{\exp\{-i\bar{H}\tau\}I_{iz}\exp\{i\bar{H}\tau\}S_{jz}\}, \tag{7}$$

where the integral is over all possible crystal orientations. These intensities form the individual proton–carbon LG-CP buildup curves. The sum of these curves along the proton chemical shift dimension, i.e., the sum of all buildup curves originating from different protons and contributing to the same carbon, corresponds to the S_j-signals measured in 1D LG-CP MAS experiments $(t_1=0)$ as

$$S_j(\omega_j^S;\tau)=\sum_i S_{ij}(\omega_i^I,\omega_j^S;\tau). \tag{8}$$

The spin pair interaction terms $\bar{H}_{ij}$ of the dipolar Hamiltonian in Eq. (6) with one common spin index do not commute with one another. As a result, the propagator governing the polarization transfer between the I_i and S_j spins cannot be factorized and the full $\bar{H}$ Hamiltonian must be diagonalized to calculate Eq. (7). In natural abundance samples these proton–carbon polarization cross-peak intensities of powder samples can be evaluated by considering only a small number of the nearest neighboring protons of each carbon. In fully ^{13}C-enriched compounds, the situation is more complicated, and a comprehensive description of the multispin dynamics may require calculations involving large spin clusters. It turns out, however, that in this case the main features of the LG-CP polarization transfer process can still be explained considering small spin systems and can be evaluated analytically or with the use of perturbation theory.

In the following sections we will discuss some LG-CP experiments on small spin systems. First we will consider the three-spin system $\{^{13}\mathrm{CH}-^{13}\mathrm{C}\}$, and then highlight some significant changes in the spin dynamics, when a proton is added as in the $\{^{13}\mathrm{CH}-^{13}\mathrm{CH}\}$ and $\{^{13}\mathrm{CH_2}-^{13}\mathrm{C}\}$ spin systems. Finally, the influence of the off-resonance term in the Hamiltonian in Eq. (6) will be discussed. The forthcoming calculations are presented in some detail in order to provide basic insight into the LG-CP spin-dynamics. For simplicity, we have assumed that all interactions in the Hamiltonian in Eq. (6) are real. The actual experimental results will, however, be analyzed by numerical simulations, taking into account all experimental parameters.

B. The three-spin system $\{^{13}\mathrm{CH}-^{13}\mathrm{C}\}$

Let us consider a ^{13}C atom next to a ^{13}CH group and ignore the proton off-resonance term in the three-spin average Hamiltonan $\bar{H}$ in Eq. (6). The influence of this term will be discussed at a later stage. For simplicity we will also assume that the dipolar coefficients d_{ij} are real. At one of the Hartmann–Hahn conditions this Hamiltonian for $\{^{13}\mathrm{C}^{(1)}\mathrm{H}^{(1)}-^{13}\mathrm{C}^{(2)}\}$ can be written as

$$\bar{H}=H_{11}+H_{12}=d_{11}(I^+S_1^-+I^-S_1^+)+d_{12}(I^+S_2^-+I^-S_2^+), \tag{9}$$

where d_{11} and d_{12} denote the effective heteronuclear dipolar couplings between the proton and carbon-1 and carbon-2, respectively. To conveniently represent this Hamiltonian, we rewrite it in terms of the fictitious spin-1/2 operators[29,30] defined in the basis set of eight product states,

$$\begin{aligned}&|1\rangle=|\alpha_\mathrm{H}\alpha_1\alpha_2\rangle\ \ |2\rangle=|\alpha_\mathrm{H}\beta_1\alpha_2\rangle\ \ |3\rangle=|\beta_\mathrm{H}\alpha_1\alpha_2\rangle\\ &|4\rangle=|\alpha_\mathrm{H}\alpha_1\beta_2\rangle\quad |5\rangle=|\beta_\mathrm{H}\alpha_1\beta_2\rangle\ \ |6\rangle=|\alpha_\mathrm{H}\beta_1\beta_2\rangle\\ &|7\rangle=|\beta_\mathrm{H}\beta_1\alpha_2\rangle\quad |8\rangle=|\beta_\mathrm{H}\beta_1\beta_2\rangle,\end{aligned} \tag{10}$$

and Eq. (9) becomes

$$\bar{H}=2d_{11}(I_x^{23}+I_x^{56})+2d_{12}(I_x^{34}+I_x^{67}). \tag{11}$$

The exact diagonalization of this Hamiltonian and the calculation of the carbon signals are carried out in the EPAPS material.[33] It is, however, more instructive to transform the Hamiltonian into a frame in which one of the two-spin terms becomes diagonal. When the proton is closer to carbon-1 than to carbon-2, we can expect that in most of the crystallites $d_{11}>d_{12}$. It is then convenient to diagonalize $\bar{H}_{11}$ first and treat $\bar{H}_{12}$ as a perturbation.

The diagonalization of $\bar{H}_{11}$ is readily accomplished by applying a rotation defined by an operator $D=\exp\{-i\pi/2(I_y^{23}+I_y^{56})\}$. In this new frame the Hamiltonian gets the form,

$$\bar{H}=2d_{11}(I_z^{23}+I_z^{56})+\sqrt{2}d_{12}(I_x^{34}+I_x^{67}+I_x^{24}+I_x^{57}), \tag{12}$$

where the states $|2\rangle,|3\rangle$ and $|5\rangle,|6\rangle$ become the linear combinations of the product spin states $1/\sqrt{2}\{|2\rangle\pm|3\rangle\}$ and $1/\sqrt{2}\{|5\rangle\pm|6\rangle\}$, respectively. The d_{11} part of the Hamiltonian becomes diagonal, whereas all elements proportional to d_{12} remain off-diagonal. The energy levels of this Hamiltonian are shown schematically in Fig. 2, with $E_1=E_4=E_7=E_8=0$ and $E_2=E_5=-E_3=-E_6=d_{11}$. In this new representation the operator corresponding to proton polarization, representing the initial state of the system, becomes partially off-diagonal

$$I_z'=I_z^{18}+I_z^{47}-I_x^{23}+I_x^{56}, \tag{13}$$

and so does the operator representing polarization of the first carbon

$$S_{1z}'=I_z^{18}+I_z^{47}+I_x^{23}-I_x^{56}. \tag{14}$$

The contributions I_x^{23}, I_x^{56} do not commute with the diagonal part of the Hamiltonian and will lead to the oscillation terms determined by the d_{11} dipolar coupling alone. This is schematically represented in Fig. 2(a). The polarization operator of the second carbon commutes with the transformation operator D, and therefore remains the same

$$S_{2z}'=I_z^{34}+I_z^{25}+I_z^{18}-I_z^{67}. \tag{15}$$

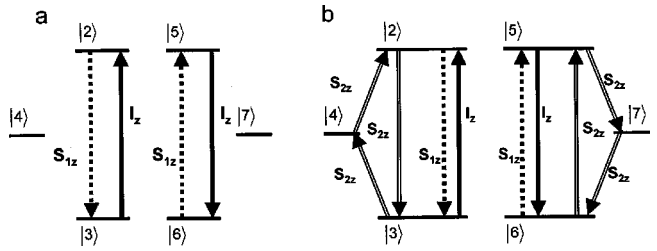

FIG. 2. An energy level diagram demonstrating the perturbation theory treatment of the three-spin system $\{^{13}C^{(1)}H^{(1)}-^{13}C^{(2)}\}$ with a Hamiltonian given in Eq. (11). The energy level diagram shown in (a) represents the Hamiltonian in the eigenbasis set of the strong $^{13}C^{(1)}-H^{(1)}$ interaction. The solid and dashed arrows show off-diagonal elements of the proton I_z' and carbon S_{1z}' polarization operators, as explained in the main text, respectively. The direction of the arrows corresponds to the sign of the represented element d At this stage, the weaker dipolar interaction is neglected and no $^{13}C^{(2)}$ signal is generated. In (b) this weaker dipolar interaction is treated as a perturbation. The energy levels shift according to the Hamiltonian in Eq. (16), and the polarization operators acquire corrections of the order of $(d_{12}/d_{11})^2$. In particular, the S_{2z}' operator acquires coherences shown by the double arrows. Signals of both carbons will oscillate with the same frequency $2(d_{11}+d_{12}^2/2d_{11})$ and the amplitudes will be proportional to $\sim(d_{12}/d_{11})^2$ The states $|1\rangle$ and $|8\rangle$ are not coupled to any other states and therefore are not shown in the diagram.

Obviously, it commutes with the dominant diagonal part of the Hamiltonian in Eq. (12) and no polarization is generated on the second carbon.

The off-diagonal terms in Eq. (12) have a minor influence on the diagonalization of the Hamiltonian when $d_{12} \ll d_{11}$. Taking into account only the first nonvanishing correction, the Hamiltonian can be approximated by

$$\bar{H}=2\left(d_{11}+\frac{d_{12}^2}{2d_{11}}\right)(I_z^{23}+I_z^{56}). \tag{16}$$

This same perturbation creates corrections to all three polarization operators in Eqs. (13)–(15). The magnitudes of these corrections are proportional to the square of the ratio of the dipolar couplings d_{12}^2/d_{11}^2. The corrected S_{2z}' operator has off-diagonal elements connecting states 2 and 3, 5 and 7, as well as 4 with 2 and 3, and 7 with 5 and 6, as shown in Fig. 2(b). They do not commute with the Hamiltonian in Eq. (16), and will acquire a time dependence. The operators I_z' and S_{1z}' stay almost intact, with off-diagonal elements between 2 and 3, and 5 and 7. Thus only off-diagonal elements between 2 and 3, and 5 and 7 contribute to the time-dependent part of the observables, resulting in signals oscillating with the same frequency, $2(d_{11}+d_{12}^2/2d_{11})$, for both carbons. The amplitude of the oscillation in the signal time dependence will be proportional to the squared ratio of the dipolar couplings.

In the EPAPS material, the exact expressions for the two carbon signals for a crystallite, with an orientation defined by a set of Euler angles Ω, are calculated analytically, with the results;

$$\begin{aligned} S_1(\tau)/S_0^{(1)}&=\frac{\gamma_I}{4\gamma_S}(1+\cos 2\varphi(\Omega))\{1-\cos 2\bar{d}(\Omega)\tau\},\\ S_2(\tau)/S_0^{(2)}&=\frac{\gamma_I}{4\gamma_S}(1-\cos 2\varphi(\Omega))\{1-\cos 2\bar{d}(\Omega)\tau\} \end{aligned} \tag{17}$$

with

$$\bar{d}(\Omega)=\sqrt{d_{11}^2+d_{12}^2}\ \text{ and }\ \tan\varphi(\Omega)=\frac{d_{12}}{d_{11}}. \tag{18}$$

The signals are normalized with respect to $S_0^{(i)}$: the intensities of the carbon signals after a single $\pi/2$ excitation pulse. Both signals oscillate with the same frequency. The important feature of Eq. (17) is that not only the signal frequencies depend on the dipolar couplings but their amplitudes as well. The ratio between these amplitudes $R=(1+\cos 2\varphi(\Omega))/(1-\cos 2\varphi(\Omega))=d_{11}^2/d_{12}^2$ is a function of the relative magnitudes of the effective dipolar interactions for a given crystalline orientation. When the spin configuration corresponds to a ^{13}C (carbon-2) weakly coupled to a ^{13}CH group (carbon-1), with $d_{11}\gg d_{12}$, $\varphi(\Omega)$ tends to zero and almost all polarization goes to the first carbon. This leaves the second carbon only weakly polarized, as predicted by perturbation theory. In the intermediate case when $d_{11}\approx d_{12}$ the total intensity is shared almost equally between the two carbons. In a powder sample the ratio between the leveling-off values of the carbon signals is a function of its structural conformation. It has a complex dependence on the proton–carbon distances and the relative orientations of the dipolar vectors. In a collinear conformation this ratio is proportional to the sixth power of the distance ratio, whereas for other conformations this power is <6.

The proton polarization oscillates during the mixing time according to

$$\begin{aligned} S^H(\tau)/S_0^H&=\mathrm{Tr}(\exp\{-i\bar{H}\tau\}I_z\exp\{i\bar{H}\tau\})\\ &=\tfrac{1}{2}(1+\cos 2\bar{d}(\Omega)\tau). \end{aligned} \tag{19}$$

This signal is independent of the φ -angle and oscillates with the same frequency $2\bar{d}(\Omega)$ as the carbon signals.

The time dependence of the carbon LG-CP signals in Eq. (17) is a result of the coherent evolution of the spin system. Furthermore, this result shows that a carbon located close to a proton reduces the amount of proton polarization being transferred to other and more remote carbons. To verify this conclusion, we performed exact powder simulations for two model spin systems: (i) a carbon–proton spin pair, $\{H-^{13}C^{(2)}\}$ with a carbon–proton distance of ~ 2.1 Å, and (ii) the same carbon–proton pair with the addition of a carbon close to the proton $\{H^{13}C^{(1)}-^{13}C^{(2)}\}$ with a $H-^{13}C^{(1)}$ separation of only ~ 1 Å. The signals of carbon $^{13}C^{(2)}$ are plotted in Fig. 3. In the spin pair case the carbon polarization reaches a value approaching $0.5\gamma_I/\gamma_S$. The amount of polarization transferred to this carbon is much reduced when another strongly coupled carbon is added to the spin system. We can therefore expect that the $H-^{13}C^{(1)}$ cross peak in a LG-CP 2D HETCOR spectrum will be much stronger than the $H-^{13}C^{(2)}$ cross peak.

C. The four spin system $\{^{13}CH-^{13}CH\}$

The situation changes when two ^{13}CH groups are coupled like in the $\{^{13}C^{(1)}H^{(1)}-^{13}C^{(2)}H^{(2)}\}$ system. Here, two additional heteronuclear proton–carbon interaction terms must be added to the d_{11} and d_{12} interactions in Eq.

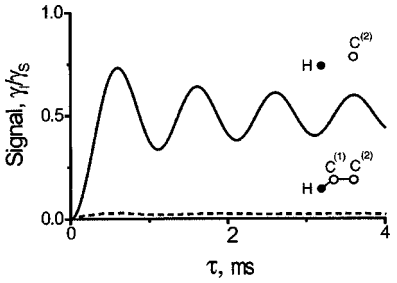

FIG. 3. Simulated powder LG-CP buildup curves of $^{13}C^{(2)}$ calculated for a $\{^{13}C^{(2)}-H^{(1)}\}$ two-spin (solid line) and a $\{^{13}C^{(1)}H^{(1)}-^{13}C^{(2)}\}$ three-spin system (dashed line). In the calculations the distance between $^{13}C^{(1)}$ and $H^{(1)}$ was 1 Å, between $^{13}C^{(2)}$ and $H^{(1)}$ it was 2.1 Å, and the $^{13}C^{(1)}-^{13}C^{(2)}$ distance was 1.5 Å.

(11) with coefficients d_{21} between $H^{(2)}$ and $^{13}C^{(1)}$ and d_{22} between $H^{(2)}$ and $^{13}C^{(2)}$. Because of the complexity of the spin system the evaluations of the carbon signals must be calculated numerically. An approximate solution can, however, be obtained assuming that the dipolar couplings $d_{11}=d_{22}=D$ are equal, as well as $d_{12}=d_{21}=d$, and that $D \gg d$. This is elaborated in the EPAPS material. For this special case the contributions of the $H^{(1)}$ proton polarization to both carbon signals, derived in the EPAPS material, are simply given by the expressions,

$$H^{(1)} \rightarrow {}^{13}C^{(1)}:$$

$$S_1(\tau)/S_0^{(1)} = \frac{\gamma_I}{8\gamma_S}(1-\cos 2D\tau)(3+\cos 2d\tau),$$

$$H^{(1)} \rightarrow {}^{13}C^{(2)}: \tag{20}$$

$$S_2(\tau)/S_0^{(2)} = \frac{\gamma_I}{8\gamma_S}(1+\cos 2D\tau)(1-\cos 2d\tau).$$

In contrast to the three-spin case, the amplitudes of the signals are not explicit functions of the dipolar couplings. The short time scale behavior of the cross peak intensities is determined by the ''active'' dipolar coupling of the heteronuclear spin pairs, corresponding to the specific cross peak. We therefore expect that the initial buildup will be slower for the $H^{(1)}-C^{(2)}$ than for the $H^{(1)}-C^{(1)}$ peak intensity. At longer times both couplings become important and both cross peaks can reach comparable intensities when $d_{11} \cong d_{22}$ and $d_{12} \cong d_{21}$. This is demonstrated in Fig. 4, where the signals of the three-spin $\{^{13}C^{(1)}H^{(1)}-^{13}C^{(2)}\}$ system are compared with the signals of two four-spin systems $\{^{13}C^{(1)}H^{(1)}-^{13}C^{(2)}H^{(2)}\}$. As was previously discussed, in the three-spin system almost all proton $H^{(1)}$ polarization is transferred to the strongly coupled carbon $^{13}C^{(1)}$. When a proton is added to this system in such a way that the $\{^{13}C^{(1)}H^{(1)}-^{13}C^{(2)}H^{(2)}\}$ spin quartet is in a *trans*-conformation, as in Fig. 4(c), the initial buildup is much slower for the cross peak of the weakly coupled pair $^{13}C^{(2)}H^{(1)}$ than for the $^{13}C^{(1)}H^{(1)}$ cross peak. However, both peaks reach about the same saturation level, as predicted in Eq. (20). When the spin system is in the *cis*-conformation, as in Fig. 4(b), the strongly coupled carbon of $^{13}C^{(1)}H^{(1)}$ again dominates the buildup, whereas the $^{13}C^{(2)}H^{(1)}$ cross peak

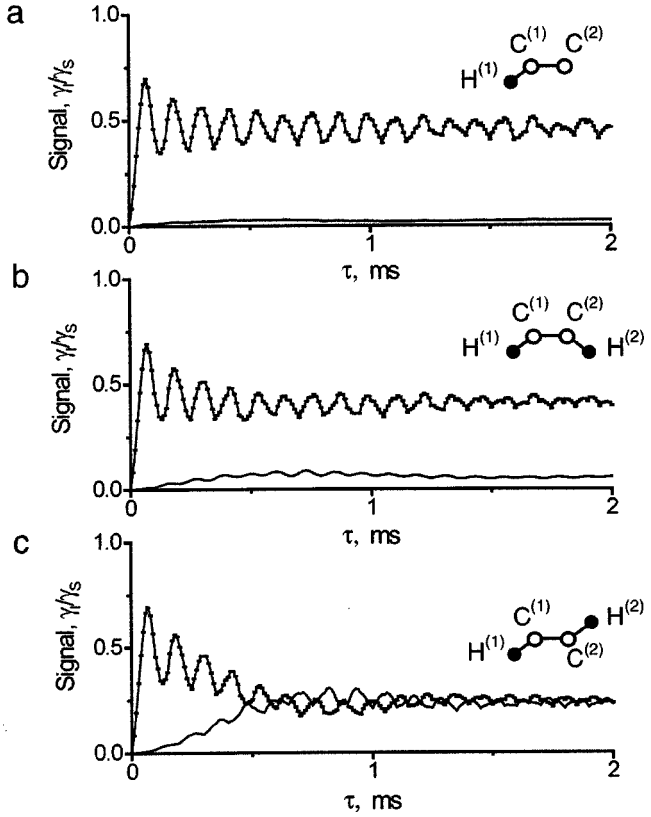

FIG. 4. Simulated powder LG-CP buildup curves for the four-spin system $\{^{13}C^{(1)}H^{(1)}-^{13}C^{(2)}H^{(2)}\}$ with geometries shown in the figures. In all simulations only the $H^{(1)}$ proton is initially polarized. The solid line with squares represents the signal corresponding to $C^{(1)}$, and the solid line alone corresponds to $C^{(2)}$. In (a) the signals of the two carbons in a three-spin system are shown ($d_{21}=d_{22}=0$), and in (b) (c) the effects on the signals due to the additional proton in a *cis*- (b) and a *trans*- (c) conformation are shown.

intensity stays small in contrast to Eq. (20). The difference between Figs. 4(b) and 4(c) can be explained by the fact that in the *cis*-conformation the d_{11} and d_{22} coupling strengths are hardly ever equal in polycrystalline samples, whereas in the *trans*-configuration they are always equal. Thus Eq. (20) only describes the latter geometry. The difference between the leveling off values of the peaks is thus dependent on the configuration of the spin system. The symmetry of the spin systems predicts that the $^{13}C^{(2)}H^{(2)}$ and $^{13}C^{(1)}H^{(2)}$ cross peaks exhibit the same time dependence, as the $^{13}C^{(1)}H^{(1)}$ and $^{13}C^{(2)}H^{(1)}$ cross peaks in Eq. (20). Thus the buildup curves of the two carbons in 1D LG-CP experiments are the same and are equal to the sum of the two curves in Figs. 4(b) and 4(c).

D. The four-spin system $\{H_2\,{}^{13}C-{}^{13}C\}$

In Fig. 5 we compare the powder buildup curves of a $^{13}C^{(2)}$ nucleus bound to a $^{13}CH_2$ group and of the $^{13}C^{(1)}$ carbon of the $^{13}CH_2$ group itself. Significant $^{13}C^{(2)}$ carbon polarization is generated in both instances, in contrast to the polarization of $^{13}C^{(2)}$ next to a ^{13}CH group. To understand these results, we can perform an approximate calculation to demonstrate the cross-polarization between the protons of $^{13}C^{(1)}H_2$ and a neighboring $^{13}C^{(2)}$ in $\{^{13}C^{(1)}H_2^{(1,2)}-^{13}C^{(2)}\}$. To simplify this calculation, we have assumed (in reality they

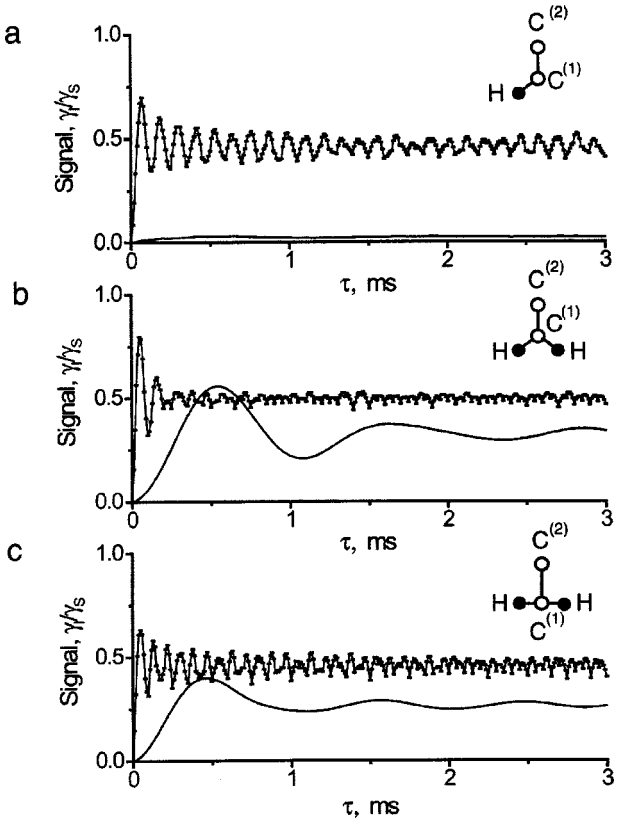

FIG. 5. Simulated powder LG-CP buildup curves calculated for a four-spin system $\{^{13}C^{(1)}H_2-^{13}C^{(2)}\}$ with geometries shown in the figures. The solid lines with squares represent signals corresponding to $^{13}C^{(1)}$, and the solid lines to $^{13}C^{(2)}$. In (a) the signals of the two carbons in a three-spin system are shown, and in (b) and (c) the effects of the additional proton in the non-collinear (b) and collinear (c) ($H-^{13}C^{(1)}-H$) conformation are shown. The carbon–proton $C^{(1)}-H^{(1,2)}$ and $C^{(2)}-H^{(1,2)}$ distances were kept constant with the $C^{(1)}-H^{(1)}$ and $C^{(1)}-H^{(2)}$ distances equal to 1 Å and the $C^{(2)}-H^{(1)}$ and $C^{(2)}-H^{(2)}$ distances are 2.1 Å. The proton–proton interactions were set to zero in order not to mix the effects due to residual proton–proton dipolar interactions and the effects generated by the heteronuclear effective Hamiltonian.

differ because of their orientation dependence) that the interaction coefficients d_{CH} between the carbons and the protons in the spin system are equal, $d^{(1)}=d_{11}=d_{21}$ and $d^{(2)}=d_{12}=d_{22}$, where again d_{11}, d_{21} and d_{21}, d_{22} denote dipolar couplings between spins $^{13}C^{(1)}$ and $H^{(1,2)}$, and $^{13}C^{(2)}$ and $H^{(1,2)}$, respectively. The following discussion provides, therefore, only a physical insight into the spin dynamics of the LG-CP process, and cannot be used for actual data analysis. An explicit derivation of the buildup curves is given in the EPAPS material.

In a single crystallite the LG-CP buildup curve for $^{13}C^{(1)}$ and the depletion of the proton signals in the three-spin system $\{^{13}C^{(1)}H_2^{(1,2)}\}$ ($d^{(2)}=0$) become, respectively,

$$\begin{aligned} S_1(\tau)/S_0^{(1)} &= \frac{\gamma_I}{2\gamma_S}(1-\cos 2\sqrt{2}d^{(1)}\tau), \\ S^{H_2}(\tau)/S_0^{H_2} &= \tfrac{1}{4}(3+\cos 2\sqrt{2}d^{(1)}\tau). \end{aligned} \tag{21}$$

In this three-spin system only half of the proton polarization of H_2 participates in the LG-CP process. Thus, in a powder the buildup curve of $^{13}C^{(1)}$ will reach an average value that is equal to its equivalent in the two-spin system $\{^{13}C^{(1)}H^{(1)}\}$.

As a result, the $^{13}C^{(2)}$ in the $\{^{13}C^{(1)}H^{(1,2)}-^{13}C^{(2)}\}$ spin system can be polarized by the H_2 protons even when $d^{(1)} \gg d^{(2)}$. This is demonstrated in detail in the EPAPS material, where the LG-CP signals of $^{13}C^{(1)}$ and $^{13}C^{(2)}$ are derived. When for simplicity we still assume that $d_{11}=d_{21}$ and $d_{12}=d_{22}$, the single crystal results are, according to the EPAPS material,

$$\begin{aligned} S_1(\tau)/S_0^{(1)} &= \frac{\gamma_I}{2\gamma_S}(1-\cos 2\sqrt{2}d^{(1)}\tau), \\ S_2(\tau)/S_0^{(2)} &= \frac{\gamma_I}{4\gamma_S}(1-\cos 2\sqrt{2}d^{(2)}\tau), \end{aligned} \tag{22}$$

and

$$S^{H_2}(\tau)/S_0^{H_2} = \tfrac{1}{8}(5+2\cos 2\langle^{(1)}\tau+\cos 2\sqrt{2}d^{(2)}\tau). \tag{23}$$

Powder integration yields polarizations on both carbons, despite the large difference between the two interaction strengths. This is demonstrated in Fig. 5(c), where simulated buildup curves for this simplified spin system are shown. Only numerical calculations can provide us with theoretical LG-CP buildup curves for more realistic parameters, as shown in Fig. 5(b). In experiments involving $^{13}CH_2$ groups, the effective interactions between the carbon and its two protons in a crystallite are not equal and the spin evolution is expected to be more complicated. However, the fact that not all H_2 proton polarization is transferred to their nearest neighboring carbon is still valid, as well as the polarization transfer to more remote carbons. Results from numerical simulations in Fig. 5(b) demonstrate this effect very clearly.

E. Off-resonance effects

Up to this point we have ignored the offset terms in the average interaction Hamiltonian in Eq. (6). We pointed out previously that the offset terms reintroduce some small effective homonuclear proton–proton interactions. However, the effect of these interactions on the spin dynamics of the LG-CP polarization exchange is small[12] and can be ignored. Following the derivation of Eq. (6) a proton with an off-resonance value of $\Delta\omega_i$ contributes a term $(\Delta\omega_i-\Delta\omega)\cos\theta_m I_{iz}$ to the average interaction Hamiltonian. These terms can become significant when they are of the same order or larger than the effective heteronuclear interaction strengths. To understand their effects on the spin dynamics, it is sufficient to consider a two-spin $^{13}CH^{(1)}$ system subjected to the proton off-resonance term,

$$\bar{H} = 2d(I^+S^- + I^-S^+) + \Delta I_z. \tag{24}$$

Here the dipolar interaction term of Eq. (6) is replaced by a real coefficient d and $\Delta=(\Delta\omega_1-\Delta\omega)\cos\theta_m$. During the LG-CP mixing time the carbon polarization increases as a function of time according to[31]

$$S(\tau)/S_0 = \frac{\gamma_I}{2\gamma_S}\sin^2\Theta(1-\cos\bar{d}\tau) \tag{25}$$

with

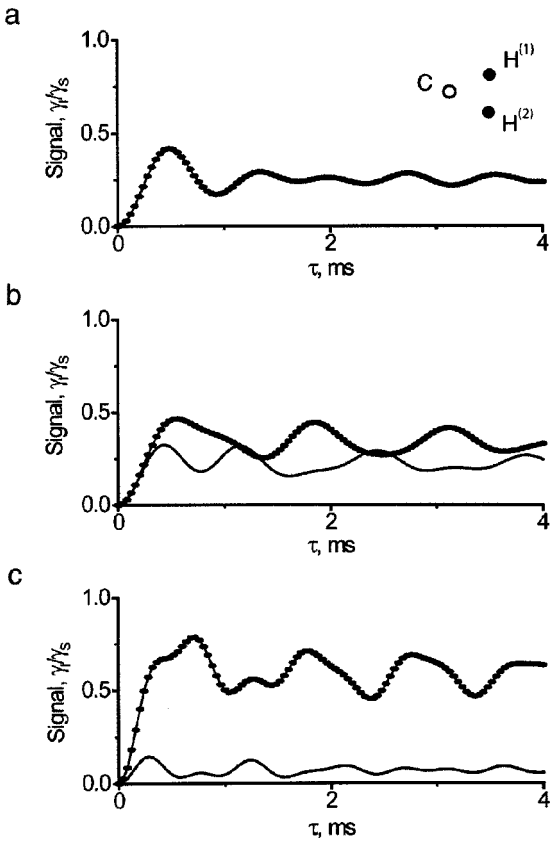

FIG. 6. Simulated powder LG-CP buildup curves calculated for the carbon in a $\{H^{(1)}-{}^{13}C-H^{(2)}\}$ system as a function of the off-resonance value of the $H^{(2)}$ proton. In the calculations the $C-H^{(1,2)}$ distances were the same and equal to 2.1 Å. The $H^{(1)}$ proton was kept on resonance. In (a) the $H^{(2)}$ proton is on-resonance, in (b) at an off-resonance value of $\Delta\omega_2=1$ kHz and in (c) at 2.5 kHz.

$$\bar{d}=\sqrt{d^2+\Delta^2} \quad \text{and} \quad \tan\Theta=\frac{d}{\Delta}.$$

As long as the dipolar coupling is larger than the offset term, $d\gg\Delta$, its effect will be relatively small. However, when the offset exceeds the dipolar coupling, $\Delta\geqslant d$, the amplitude of the oscillation described by Eq. (25) decreases, whereas the frequency increases.

The situation is similar in larger spin systems. As an example, we considered a three-spin $(H^{(1)}-{}^{13}C-H^{(2)})$ system consisting of two protons and one carbon. In Fig. 6 the two carbon buildup curves originating from $H^{(1)}$ and $H^{(2)}$ as a function of the offset of $H^{(2)}$ are shown. When the offset is set to zero, both buildup curves are identical since the protons are identical. When the offset value becomes comparable with the dipolar interaction between the $H^{(2)}$ proton and the carbon, the $H^{(2)}\rightarrow{}^{13}C$ polarization transfer gets reduced. When the offset is much larger than the dipolar interaction, the $H^{(2)}$ proton does not participate in the spin dynamics, since the effective field for this proton does not satisfy the Hartmann Hahn condition, and the spins behave like an isolated $^{13}CH^{(1)}$ spin pair.

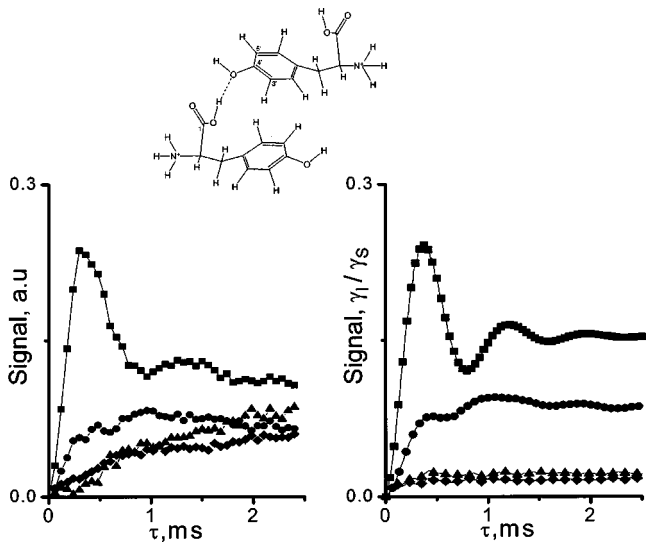

FIG. 7. The arrangement of two molecules in crystalline L-tyrosine.HCl, according to neutron diffraction data (Ref. 32) with the intermolecular hydrogen bonding indicated by the dashed line. The experimental and calculated LG-CP buildup curves of the 4′-^{13}C carbon recorded by 3D LG-CP experiments, and originating from the 1-OOH (circles), 4′-OH (squares), 3′-H (upper triangles), and 5′-H (diamonds) protons, are shown in (a) and (b), respectively. The experimental data were scaled to equalize the maximum intensity of the 4′-OH buildup curve with the corresponding simulated one.

IV. RESULTS AND DISCUSSION

A. [U−^{13}C] tyrosine.HCl

LG-CP experiments were performed on a sample of [U−^{13}C] tyrosine.HCl. The results presented below have been published earlier, but were not analyzed explicitly.[11] We will therefore focus on the analysis of these results in the framework of the theory represented in the previous section. In particular, we will discuss the polarization transfer processes taking place between the 4′-^{13}C carbon and its nearest four protons. According to neutron diffraction data, these four protons are the 4′-OH phenolic proton, 1.982 Å away from 4′-^{13}C, the two aromatic protons 3′-H and 5′-H at 2.150 and 2.148 Å, respectively, and the 1-OOH proton of a neighboring molecule in the crystal at 2.521 Å. The latter is the hydrogen bonding proton formed by the 4′ hydroxyl group and the 1-OO^-. The crystal arrangement is shown in Fig. 7.

The individual polarization transfer curves of 4′-^{13}C were extracted from the 3D LG-CPMAS experiment shown in Fig. 1(b). The intensities of the cross peaks, shown in Fig. 7(a), are a function of the LG-CP mixing time τ. The polarization from the 4′-OH proton shows a fast buildup with a maximum at about 0.4 ms. In contrast, the buildup curves from the 3′-H and 5′-H protons are much slower and less effective, despite the fact that the distances between these protons and the 4′-^{13}C carbon are similar to that between 4′-OH and 4′-^{13}C. These data can be qualitatively understood by comparing their spin dynamics with that of the simplified three-spin model described in the previous section. The interactions of the aromatic protons with their directly bonded carbons ($r\sim1$ Å) are much stronger than their interactions with the remote 4′-^{13}C. Accordingly, the

(3′-H)–(3′-^{13}C) and (5′-H)–(5′-^{13}C) spin systems behave like isolated spin pairs and only a very small fraction of the proton magnetization can be transferred to the 4′-^{13}C. However, the 4′-OH does not have a directly bonded ^{13}C and its proton magnetization will be transferred to the 4′-^{13}C. Thus, the polarization transfer between the 4′-^{13}C and 4′-OH becomes similar to a two-spin system. The interactions between the 4′-^{13}C and 4′-OH spins and more remote spins come into play at a longer time scale and bring about a leveling off of the signal similar to the effects observed for the natural abundant ^{13}C in alanine.[12] The polarization from the 1-OOH proton builds up slowly and reaches a value somewhat smaller than that from the 4′-OH proton. In addition to being farther away from the 4′-^{13}C than the 4′-OH, this proton has a 1-^{13}C, which is relatively close (1.886 Å). Therefore, the polarization transfer process between the 1-OOH and the 4′-^{13}C is partially truncated by its stronger (1-OOH)-(1-^{13}C) interaction.

The theoretical curves in Fig. 7(b) were calculated by taking into account the real geometry of the system. wo spin systems consisting of six spins each: {4′-OH,1-OOH,4′-^{13}C,1-^{13}C,3′-H,3′-^{13}C} and {4′-OH,1-OOH,4′-^{13}C,1-^{13}C,5′-H,5′-^{13}C} were considered. The simulated build-up curves corresponding to 4′H $\rightarrow$4′-^{13}C and 1-OOH$\rightarrow$4′-^{13}C were multiplied by exponential decay functions with a decay rate of 1.4×10^{3} s^{-1} and 5×10^{2} s^{-1}, respectively. As can be seen in Fig. 7, the agreement between the experiment and the simulation is quite satisfactory, in particular the values of the frequencies of oscillations. Some of the discrepancies, in particular, the decay of the 4′-H$\rightarrow$4′-^{13}C curve and the increase of the 3′-H$\rightarrow$4′-^{13}C and 5′-H$\rightarrow$4′-^{13}C curves, must be attributed to multispin interactions in the sample and Hartmann–Hahn mismatches due to RF inhomogeneities. These effects are of course not taken into account during six-spin simulation. They should also be responsible for the decay of the oscillations, introduced in the simulations by the above mentioned decay rates. Thus the complexity and the size of the system allow only qualitative analysis of whole experimental data. However, the oscillations that are mainly due to short distance interactions can be attributed to local conformations. Overall, the experimental data support the conclusions of the Theory.

B. [U–^{13}C, ^{15}N] histidine.HCl

The interpretation of the LG-CP buildup curves of the quaternary (4-^{13}C) carbon in [U–^{13}C, ^{15}N]–histidine.HCl.H_2O sample represents a much more challenging problem. Here, both the effects typical for {$^{13}CH_2-^{13}C$} spin systems and the offset effects discussed in the Theory become evident. In addition, a relatively large number of spins participate in the spin dynamics and they all should be taken into account in the simulations. Figure 8 presents the molecule schematically. The quaternary carbon does not have directly bonded protons and is approximately equidistant from the proton of the ring nitrogen (2-^{15}N), and from the two protons of the C_β carbon. Both proton–carbon interaction strengths are about 3 kHz. However, these $^{13}CH_2$ and

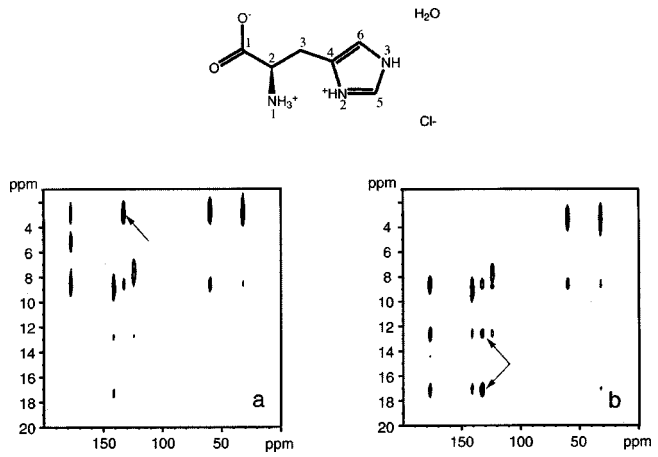

FIG. 8. The structure of [U-^{13}C, ^{15}N] histidine.HCl.H_2O and 2D heteronuclear correlation spectra obtained from the experiment shown in Fig. 1(b) with $\tau=0.8$ ms. The spectrum in (a) results from an experiment in which the polarization transfer efficiency between the protons of C_β and 4-^{13}C was maximized. An arrow points to the corresponding cross peak. The cross peak intensities corresponding to 2-^{15}NH and 3-^{15}NH with 4-^{13}C are below the contour limits. In 2D LG-CP spectrum in (b) the proton carrier frequency was moved and the cross peaks between the 2-^{15}NH and 3-^{15}NH protons and 4-^{13}C become stronger (indicated by arrows), whereas the polarization transfer with the protons of $^{13}CH_2$ is significantly reduced.

^{15}NH protons have different isotropic chemical shifts and the efficiency of the polarization transfer, originating from these protons, is expected to be strongly dependent on the exact position of the proton carrier frequency. Figure 8 shows the 2D heteronuclear correlation spectra obtained with different carrier positions. In Fig. 8(a) the proton RF frequency was chosen to maximize the transfer from the $^{13}CH_2$ protons. The cross peak between the $^{13}CH_2$ protons and the 4-^{13}C carbon is present in the spectrum and indicated by an arrow. The three cross peaks, corresponding to the cross polarization from the 2-^{15}NH proton, the 3-^{15}NH proton, and the $^{15}NH_3$ protons to the quaternary carbon 4-^{13}C are diminished. This is further supported in Fig. 9(a), where the cross peak intensities are shown as a function of the LG-CP mixing time τ.

Clearly, most of the polarization comes from the $^{13}CH_2$ protons, despite the fact that the $^{13}CH_2$ protons are strongly coupled to their $^{13}C_\beta$-carbon. This result is in agreement with the theoretical predictions of the previous section, where the ($^{13}CH_2-^{13}C$) spin system was analyzed. The polarization transfer from other protons is markedly suppressed due to off-resonance effects as explained above. The experimental results agree well with the simulations shown in Fig. 9(b). A 9-spin system, consisting of 7 protons (CH_2, NH_3, 2-NH, and 3-NH) and 2 carbons (2-^{13}C and 4-^{13}C) was considered in this simulation. The fast exchange dynamics of the NH_3 protons was explicitly taken into account in the simulations. The values of the carbon and proton RF fields and their offset frequencies were derived from the experiment.

In a reverse experiment the proton carrier frequency is positioned to maximize the transfer from the 2-^{15}NH, 3-^{15}NH, and $^{15}NH_3$ protons to the 4-^{13}C carbon and their corresponding cross peaks are enhanced, whereas the cross peak from the $^{13}CH_2$ protons is significantly reduced, as evident from Figs. 8(b) and 9(c). The difference between the

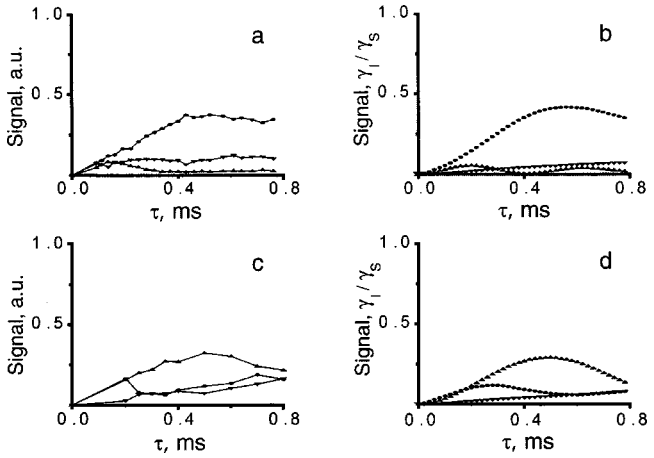

FIG. 9. The cross peak intensities extracted from 3D LG-CP experiments on [U−^{13}C, ^{15}N] histidine.HCl.H_2O and their corresponding simulations are shown. The experimental results in (a), obtained with the proton carrier frequency chosen to maximize the transfer between the 3-$^{13}CH_2$ protons and the 4-^{13}C carbon, are compared with simulations in (b). The experimental results, obtained with a proton carrier frequency that maximizes the transfer between the $^{15}NH_3$ and 2-^{15}NH protons and the 4-^{13}C carbon, are shown in (c) and must be compared with simulations in (d). The buildup curves originating from the $^{13}CH_2$ protons are drown by circles, those from the $^{15}NH_3$ protons are lower triangles, and those from 2-^{15}NH are upper triangles. The experimental data were scaled to equalize the maximum intensity of the experimental buildup curves with the corresponding simulated one.

effective fields experienced by the carbon and these $^{13}CH_2$ protons becomes larger than the effective LG-CP interaction strength, and hence the Hartmann–Hahn condition is violated. This effectively removes these protons from the spin dynamics. Figure 9(d) shows the simulated buildup curves originating from the different protons. Clearly the polarization transfer is dominated by the 2-^{15}NH proton, since it is the closest to the quaternary carbon, does not have carbons nearby, and its offset satisfies the Hartmann–Hahn condition. In contrast, the $^{13}CH_2$ protons become less involved in the spin dynamics, in agreement with the results of the theory.

V. CONCLUSIONS

We have shown that coherent processes dictate the polarization transfer spin dynamics in high spinning LG-CP experiments. The coherent effects manifest themselves in the dependence of the oscillation frequencies and the leveling-off values on the dipolar couplings. Usually, initially polarized protons transfer most of their polarizations only to the strongly coupled carbons and the polarization transfer to weakly coupled carbons is substantially reduced. An exception occurs when the CP process involves the $^{13}CH_2-^{13}C$ spin system. Here a significant portion of the $^{13}CH_2$ proton polarization can be transferred to remote carbons despite the presence of a strongly coupled carbon. This implies, from a practical point of view, that the analysis of the polarization transfer processes requires considering large spin clusters, perhaps with the exception of the strongly coupled spin pairs. The presence of discrete oscillations in the buildup curves can of course provide structural information. However, they must be analyzed carefully taking into account possible multispin conformations. Favorable cases exist where precise structural information can be obtained, and the accuracy improves when appropriate spin systems are used in computer simulations.

At this stage of development of the LG-CP methods for structural studies of peptides and proteins they provide a quantitative approach for short carbon–proton distance measurements, and a qualitative tool for estimating longer distances and multispin configurations. Comparison between the buildup curves of the labeled and nonlabeled samples can provide additional structural insight. Further simplifications of the spin dynamics by deuteration of the samples are desirable for more accurate proton–carbon distance determination. Extensions of the LG-CP approach will be necessary to improve its potential to provide accurate structural information.

Regular ''on-resonance'' CP experiments are not very sensitive to the choice of the proton carrier frequency, because high intensity RF fields on the proton channel truncate all chemical shift terms to a high degree. However, the situation is quite different in the LG-CP experiments. There, the offset terms add up with the large LG-offset term. This may change the effective field significantly, and remove the proton from the Hartmann–Hahn condition, resulting in a reduction of the polarization transfer efficiency. It remains to be seen whether by controlling offset values and spin labeling, LG-CP buildup curves can help in determining the secondary structure.

ACKNOWLEDGMENTS

The authors thank Dr. Claudiu Filip for useful discussions. This research was supported by the German–Israeli Foundation for Scientific Research and Development, and was part of the ''Ultra High Field NMR'' project of the European Commission, Contract No. BIO4-CT97-2101.

[1] A. Pines, M. G. Gibby, and J. S. Waugh, J. Chem. Phys. **59**, 569 (1973).
[2] E. R. Andrew, A. Bradbury, and R. G. Eads, Nature (London) **183**, 1802 (1959).
[3] I. J. Lowe, Phys. Rev. Lett. **2**, 285 (1959).
[4] M. Mehring, A. Pines, W-K. Rhim, and J.S. Waugh, J. Chem. Phys. **54**, 3239 (1971).
[5] A. E. Bennett, C. M. Rienstra, M. Auger, K. V. Lakshmi, and R. G. Griffin, J. Chem. Phys. **103**, 6951 (1995).
[6] D. E. Demco, J. Tegenfeldt, and J. S. Waugh, Phys. Rev. B **11**, 4133 (1975).
[7] M. H. Levitt, D. Suter, and R. R. Ernst, J. Chem. Phys. **84**, 4243 (1986).
[8] B. H. Meier, Chem. Phys. Lett. **188**, 201 (1992).
[9] D. Marks and S. Vega, J. Magn. Reson. Ser. A **118**, 157 (1996).
[10] S. Ray, V. Ladizhansky, and S. Vega, J. Magn. Reson. **135**, 237 (1998).
[11] B.-J. van Rossum, C. P. de Groot, V. Ladizhansky, S. Vega, and H. J. M. de Groot, J. Am. Chem. Soc. **122**, 3465 (2000).
[12] V. Ladizhansky and S. Vega, J. Chem. Phys. **112**, 7158 (2000).
[13] M. Lee and W. I. Goldburg, Phys. Rev. A **140**, 1261 (1965).
[14] S. R. Hartmann and E. L. Hahn, Phys. Rev. **128**, 2042 (1962).
[15] P. R. Costa, Ph.D. thesis, Massachusetts Institute of Technology, 1997.
[16] M. Hohwy, C. M. Rienstra, C. P. Jaroniec, and R. G. Griffin, J. Chem. Phys. **110**, 7983 (1999).
[17] A. Brinkmann, M. Eden, and M. H. Levitt, J. Chem. Phys. **112**, 8539 (2000).
[18] B. Luy and S. J. Glaser, J. Magn. Reson. **142**, 280 (2000).
[19] P. Hodgkinson and L. Emsley, J. Magn. Reson. **139**, 46 (1999).
[20] E. Vinogradov, P. K. Madhu, and S. Vega, Chem. Phys. Lett. **314**, 443 (1999).
[21] E. Vinogradov, P. K. Madhu, and S. Vega, Chem. Phys. Lett. **329**, 207 (2000).

[22] E. Vinogradov, P. K. Madhu, and S. Vega, J. Chem. Phys. **115**, 8983 (2001).
[23] M. Mehring and J. S. Waugh, Phys. Rev. B **5**, 3459 (1972).
[24] A. Bielecki, A. C. Kolbert, and M. H. Levitt, Chem. Phys. Lett. **155**, 341 (1989).
[25] A. G. Redfield and S. D. Kunz, J. Magn. Reson. (1969-1992) **19**, 250 (1975).
[26] M. Bak, J. T. Rasmussen, and N. C. Nielsen, J. Magn. Reson. **147**, 296 (2000).
[27] M. Veshtort and R. G. Griffin (unpublished).
[28] A. E. Bennett, R. G. Griffin, and S. Vega, in *NMR Basic Principles and Progress* Springer-Verlag, Berlin, (1994), Vol. 33.
[29] A. Wokaun and R. R. Ernst, J. Chem. Phys. **67**, 1752 (1977).
[30] S. Vega, J. Chem. Phys. **68**, 5518 (1978).
[31] L. D. Landau and E. M. Lifshitz, *Quantum Mechanics*, 3rd ed., *Course of Theoretical Physics*, edited by L. D. Landau and E.M. Lifshtitz (Pergamon, Oxford, 1981), Vol. 3.
[32] M. N. Frey, T. F. Koetzle, M. S. Lehmann, and W. C. Hamilton, J. Chem. Phys. **58**, 2547 (1973).
[33] See EPAPS Document No. E-JCPSA6-117-014245 for the LG-CP build-up curves of the carbon signals. A direct link to this document may be found in the online article's HTML reference section. The document may also be reached via the EPAPS homepage (http://www.aip.org/pubservs/epaps.html) or from ftp.aip.org. in the directory /epaps/. See the EPAPS homepage for more information.